

Photon decay in circuit quantum electrodynamics

R. Kuzmin,¹ N. Grabon,¹ N. Mehta,¹ A. Burshtein,² M. Goldstein,² M. Houzet,³ L. I. Glazman,⁴ and V. E. Manucharyan¹

¹*Department of Physics, University of Maryland, College Park, Maryland 20742, USA.*

²*Raymond and Beverly Sackler School of Physics and Astronomy, Tel Aviv University, Tel Aviv 6997801, Israel.*

³*Univ. Grenoble Alpes, CEA, INAC-Pheliqs, F-38000 Grenoble, France.*

⁴*Department of Physics, Yale University, New Haven, CT 06520, USA.*

(Dated: March 1, 2022)

Light does not typically scatter light, as witnessed by the linearity of Maxwell’s equations. We constructed a superconducting circuit, in which microwave photons have well-defined energy and momentum, but their lifetime is finite due to decay into lower energy photons. The inelastic photon-photon interaction originates from quantum phase-slip fluctuation in a single Josephson junction and has no analogs in quantum optics. Instead, the surprisingly high decay rate is explained by mapping the system to a Luttinger liquid containing an impurity. Our result connects circuit quantum electrodynamics to the topic of boundary quantum field theories in two dimensions, influential to both high-energy and condensed matter physics. The photon lifetime data is a rare example of a verified and useful quantum many-body simulation.

Although photons have zero mass, fundamental laws do not prevent their decay into more photons as soon as some form of non-linearity is present. Thus, individual 100 MeV-photons split in the Coulomb field of heavy nuclei because of vacuum polarization¹ and so do optical photons in non-linear crystals². However, the splitting probability is extremely low, which in both cases can be traced down to the small value of the fine-structure constant. Perhaps the strongest single-photon interaction effects occur in circuit quantum electrodynamics (cQED), owing to both the reduced mode volume of microwave transmission lines and the non-linearity of Josephson junctions³. Indeed, many basic quantum optical phenomena, such as vacuum Rabi oscillations⁴, photon number splitting⁵, resonance fluorescence⁶, and parametric frequency conversion^{7,8}, can be dramatically enhanced in properly designed superconducting circuits. In addition, multi-mode and ultrastrong coupling regimes were explored^{9–11}. Yet, in the absence of a classical pump, the effect of one photon on another has been limited to a conditional phase-shift¹². In this work, we report the first instance of an inelastic photon-photon interaction, taking place in a massively multi-mode cavity resonator, and manifesting as the rapid decay of a single microwave photon.

The central part of our setup is a long on-chip “telegraph” transmission line terminated by a weak Josephson junction (Fig. 1a, upper panel). Itself made of a chain of 20,000 stronger junctions, the line implements a one-dimensional vacuum with its wave impedance Z comparable to resistance quantum for Cooper pairs $R_Q = h/(2e)^2 \approx 6.5 \text{ k}\Omega$, which translates into an effective fine structure constant $\alpha = Z/R_Q$ of order unity¹³. In such a vacuum, microwave photons propagate as sound-like transverse electro-magnetic excitations of the superconducting phase field $\varphi(x, t)$, described by a quadratic Lut-

tinger liquid-like Lagrangian

$$L_0 = \frac{\hbar v}{4\pi\alpha} \int_0^l dx \left[\frac{1}{v^2} \varphi_t^2 - \varphi_x^2 + \frac{1}{\omega_p^2} \varphi_{t,x}^2 \right], \quad (1)$$

where v is the speed of light in the low-frequency limit and the photon dispersion $\omega(k) = vk/\sqrt{1 + (vk/\omega_p)^2}$ has a natural ultra-violet cutoff at $\omega_p/2\pi \approx 20 \text{ GHz}$, given by the plasma resonance of the chain junctions. The weak “impurity” junction presents a non-linear boundary at $x = 0$ to the otherwise free field $\varphi(x > 0, t)$, which results in the following total system Lagrangian:

$$L = L_0 + E_J(\Phi) \cos \varphi(x = 0, t) + \frac{\hbar^2 \varphi_t(x = 0, t)^2}{16E_C}. \quad (2)$$

The Josephson energy E_J of the weak junction is tuned by an external flux Φ using SQUID configuration, and the charging energy $E_C = e^2/2C$ is due to the oxide capacitance C . We focus on devices with $E_C \lesssim E_J$.

For $\alpha \sim 1$, the junction’s galvanic connection gives rise to a manifestly quantum mechanism of light-light coupling, not considered previously (Fig. 1b). At the semiclassical level, the junction mimics a transmon qubit¹⁵, whose resonance frequency $\omega_0 \approx ((8E_J E_C)^{1/2} - E_C)/\hbar$ is associated with oscillations of $\varphi(x = 0, t)$ inside a single Josephson well. The resonance hybridizes with the transmission line modes and acquires a linewidth, given by the classical damping rate $\Gamma = 4E_C/\pi\hbar\alpha$ ¹⁴. Extending the transmon analogy to quantum regime, we note that weak tunneling of $\varphi(x = 0, t)$ between the Josephson wells – the quantum phase-slip fluctuation^{16,17} – would make the first vibrational level sensitive to the total charge q displaced by the transmission line at $x = 0$. In contrast with capacitively-disconnected junctions, here q is a quantum variable, previously introduced as the quasicharge^{18–20}. Its static component (offset charge) is screened by the dc-capacitance of the line, while dynamical fluctuations are

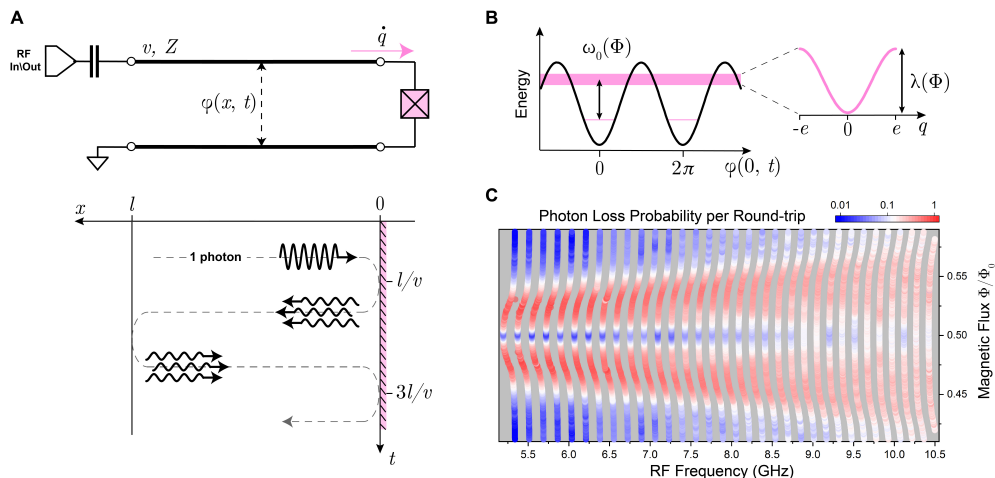


FIG. 1. (a) Circuit schematic of a telegraph transmission line terminated by a Josephson junction at the right end and weakly coupled to a measurement port at the left end. Device photographs and microwave launching setup are shown in Ref.^{13,14}. The quantum field $\varphi(x, t)$ represents the superconducting phase-difference between the two wires of the transmission line. Lower panel illustrates inelastic (elastic) scattering of photons at the junction (port) end. (b) Quantum dynamics of the boundary phase $\varphi(x = 0, t)$ in the periodic Josephson potential gives rise to a transmon-like resonance, whose frequency ω_0 is modulated by quantum fluctuations of the dynamical charge q at the end of the transmission line. (c) The measured positions of standing wave resonances as a function of flux through the impurity in device 3a. The color shows the probability to lose a photon inside the transmission line in one round-trip time.

enhanced, because the junction short-circuits the transmission line, and hence creates an antinode of current \dot{q} at $x = 0$. As a result, incident photons experience a virtual parametric pumping of the transmon resonance by quantum fluctuations of q . As the “pump” strength, given by the phase-slip rate, grows, even a single photon can efficiently down-convert (decay) into an odd number of lower-frequency photons, the choice of which is governed by energy conservation and the spectral density of quantum fluctuations of q .

More generally, inelastic scattering in our system can be considered in the context of quantum impurity physics²¹. In fact, for $E_C, \omega_p \rightarrow \infty$, the Eqs. (1,2) define the boundary sine-Gordon (BSG) quantum impurity model with a critical point at $\alpha = 1$ ²². The BSG model is notorious for its integrability property and for describing diverse condensed matter phenomena, from dissipative localization in a periodic potential^{23,24} to electron tunneling in Luttinger liquids²⁵. The critical dynamics of the field φ manifest precisely by inelastic scattering of its bulk excitations – photons in our case – off the non-linear boundary²⁶. If the scattering was limited to a mere phase-shift, the boundary could be replaced by a linear one, which would have eliminated interaction effects. Notably, calculating the reflection amplitude $r(\omega)$ as a function of frequency ω is a difficult task, and it becomes even more so in the presence of the E_C -term, which prevents using the exact BSG results. Therefore, measuring $r(\omega)$ would accomplish a useful quantum many-body simulation, which further motivates our experiment.

To measure $r(\omega)$ at $x = 0$ we introduce a second reflective boundary at $x = l = 6$ mm in the form of a weakly

coupled input/output port. A single photon impinging at the impurity boundary can either scatter elastically with a phase-shift $\delta(\omega)$ or it can split into several left-moving photons (Fig. 1a, lower panel). In both cases, the left-moving photons bounce back at $x = l$ and the process repeats. If the elastic scattering dominates, the two boundaries define a Fabry-Pérot resonator with a free spectral range $\Delta = v/(2l) \approx 150$ MHz, and the positions of standing-wave mode resonances are linked to $\delta(\omega)$. A rare inelastic event effectively annihilates the photon from a given standing-wave mode as if there is an intrinsic absorption mechanism. Consequently, Fabry-Pérot resonances would broaden by an amount $\gamma(\omega) \ll \Delta$. The quantities δ and γ are linked to r as $\ln r = 2i\delta - 2\pi\gamma/\Delta$. Thus, we reduced the scattering experiment in a practically impossible semi-infinite geometry to spectroscopy of Fabry-Pérot cavity resonances in a finite-size system.

Following the previously established rf-spectroscopy technique¹³, we identified the frequency and intrinsic linewidth of all standing-wave modes in the 5 – 10 GHz range as a function of flux Φ (Fig. 1c). The data is taken while populating the modes with much less than one quanta on average, and we checked that the spectroscopic line-shapes remained power-independent. The impurity’s resonance has no effect at an integer flux bias $\Phi = 0$, Φ_0 ($\Phi_0 = h/2e$), because then ω_0 is detuned far away towards the plasma cut-off ω_p . We used data at $\Phi_0 = 0$ to extract the dispersion relation and the value of Z , also using the methods from Ref.¹³. As ω_0 is tuned through the spectrum, multiple modes simultaneously shift by an amount comparable to Δ , signaling the achievement of superstrong coupling condition, $\Gamma \gg \Delta$ ¹⁴, required for

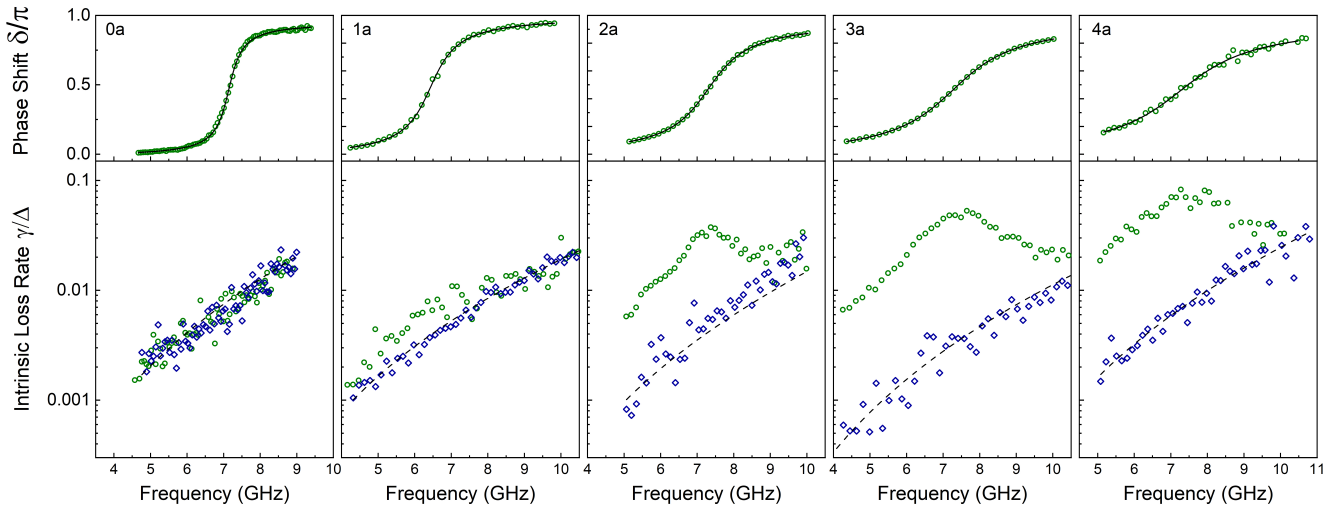


FIG. 2. The elastic (top) and inelastic parts (bottom) of the reflection amplitude $r(\omega)$ for the devices with progressively larger charging energy E_C . In each device, the flux Φ is tuned such that $\omega_0/2\pi \approx 6.5 - 7.5$ GHz. The blue markers show data at $\Phi = 0$, where the impurity is effectively switched off. The dashed line represents the background dielectric loss inside the transmission line. Device parameters are given in the Table S1 of supplementary material.

multi-mode interaction effects. The new effect, though, is an over two orders of magnitude variation of the modes linewidth γ with flux. At $\Phi/\Phi_0 \approx 0.475$, the single impurity simultaneously damps over 30 modes, spanning a considerable fraction of the entire energy window. Moreover, the value of γ near 5.5 GHz is such that photons disappear after a single collision with the impurity with a probability close to unity (Fig. 1c, deep red).

Mode by mode, we accurately extracted the elastic scattering phase δ and the intrinsic loss rate γ in ten devices with varying parameters (Table S1). The phase $\delta(\omega)$ expectedly winds by π across the impurity resonance (Fig. 2, top panels). A fit to the standard oscillator expression provides an accurate estimation of Γ and, therefore, E_C (Fig. 2, upper panel). We checked that Γ remains flux-independent while growing from 0.6 GHz in device 0a to 3.1 GHz in device 4a as the impurity junction is fabricated with progressively smaller area (larger E_C)²⁷. The loss rate is flux-independent in device 0a with $E_C = 0.39$ GHz, and it can be explained by the background dielectric absorption in Josephson transmission lines. However, already for $E_C = 0.66$ GHz in device 1a, there is a noticeable deviation of $\gamma(\omega)$ from the background at $\Phi = 0$, and this deviation rapidly grows with E_C (Fig. 2, lower panels). The anomalous dissipation is maximal for modes located in the Γ -vicinity of the impurity resonance at ω_0 , defined in Fig. 2 as $\delta(\omega_0) = \pi/2$.

Subtracting the background loss of each device from $\gamma(\omega)$, we interpret the remaining rate $\gamma_{\text{in}}(\omega)$ as the rate of photon decay due to inelastic scattering at the impurity (Fig. 3). Several properties of γ_{in} support our interpretation. The maximal decay rate $\gamma_{\text{in}}(\omega = \omega_0)$ grows by an order of magnitude on reducing $\omega_0/2\pi$ by only a few GHz. Such a strong frequency dependence of $\gamma_{\text{in}}(\omega_0)$

eliminates the possibility of mundane absorption due to either a lossy dielectric or quasiparticle tunneling in the impurity junction. In fact, the growth of $\gamma_{\text{in}}(\omega_0)$ at lower frequencies is atypical to materials loss. Furthermore, the rate $\gamma_{\text{in}}(\omega_0)$ vanishes in device 1a which features the fastest variation of ω_k with ω_0 (the sharpest function $\delta(\omega)$ near $\omega = \omega_0$ in Fig. 2). Such an observation eliminates the inhomogeneous broadening mechanism due to slow fluctuations of ω_0 in time. We have also checked that the measured port-coupling is insensitive to flux-bias, and γ_{in} is insensitive to increasing the port coupling²⁷.

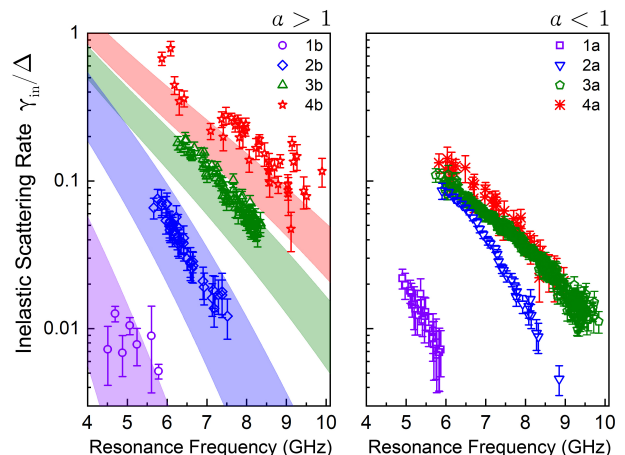


FIG. 3. Inelastic scattering rate $\gamma_{\text{in}}(\omega_0)/\Delta$ (colored markers) for devices with $\alpha > 1$ (left panel) and $\alpha < 1$ (right panel). The width of theory lines (colored bands) comes from uncertainty in the device parameters. The error bars are the standard errors of $\gamma_{\text{in}}/\Delta$ at the resonance. The color code represents nominally identical values of E_C .

Theory supports our interpretation of the anomalous dissipation in terms of photon decay²⁷. Specifically, for $\alpha > 1$, $\Gamma \ll \omega_0/2\pi$, and $E_C \ll E_J$, the observed photon decay can be quantitatively understood using the following effective phase-slip Hamiltonian,

$$H = \sum_k \hbar\omega_k a_k^\dagger a_k + \nu \cos \pi q/e, \quad (3)$$

acting at the subset of many-body states with energy near $\hbar\omega_0$. The operators a_k (a_k^\dagger) annihilate (create) photons at flux-dependent frequencies ω_k , given by positions of the spectroscopic resonances (Fig. 1c) and the effective phase-slip amplitude ν is proportional to the first Bloch band half-width λ of the isolated junction. The dynamical charge q is decomposed over the normal modes according to $q = \sum_k f_k (a_k + a_k^\dagger)$, where the factors $f_k^2 = (4\pi\Delta/\alpha\omega_k) \times \omega_0^4 / ((\omega_0^2 - \omega_k^2)^2 + (2\pi\Gamma\omega_k)^2)$ weight the contribution of individual k -modes. The non-linearity of the cosine term in Eq. 3 creates a photon-photon interaction between all the k -modes at all even orders. However, because f_k is maximal both at $\omega_k = \omega_0$ and at $k = 1$, the dominant decay products consist of one near-resonant photon and an even number of low-frequency photons. Restricting the calculation to such processes, the inelastic rate for a resonant photon can be found from the Fermi's golden rule:

$$\gamma_{in}(\omega = \omega_0)/\Delta = (\lambda/\omega_0)^2 \frac{(\pi\Gamma/\omega_0)^{2/\alpha-2}}{2(2/\alpha - 1)! \sin(\pi/\alpha)}. \quad (4)$$

Within the experimental uncertainty on model parameters, the Eq. (4) matches the data from all four devices with $\alpha > 1$ without adjustable parameters (Fig. 3a, colored bands). Either increasing E_C or reducing ω_0 with the flux-knob exponentially increases λ , which in turn causes a rapid growth of $\gamma_{in}(\omega_0)$. The effect of α is weaker, but more complex. In particular, Eq. 4 breaks down for $\alpha \rightarrow 1$, in which case photons are likely produced in the entire frequency range. Devices with $\alpha < 1$ exhibit similar, by order of magnitude, decay rates $\gamma_{in}(\omega_0)$, compared to those by devices with $\alpha > 1$ with similar values of E_C (Fig. 3a vs. Fig. 3b). However, a quantitative comparison in case $\alpha < 1$ requires more advanced theoretical models than those presently available.

To gain further insight into the photon's lifetime, we consider specific final states available for the decay of mode 47 in device 3a, with flux Φ tuned such that $\omega_0/2\pi \approx \omega_{47}/2\pi \approx 6.476$ GHz. Using extended spectroscopy data (Fig. 4, left panel), we identified those three-photon and five-photon combinations, whose frequency matches $\omega_{47}/2\pi$ within the measured linewidth $\gamma = 11$ MHz. Our construction reveals a large number of states with a relatively uniform three-photon ($\Delta^{(3)} \approx 1$ MHz) and five-photon ($\Delta^{(5)} \approx 50$ kHz) level spacing (Fig. 4, right panel). States involving higher number of photons are also available and they would form even denser spectrum. We checked that most three-photon

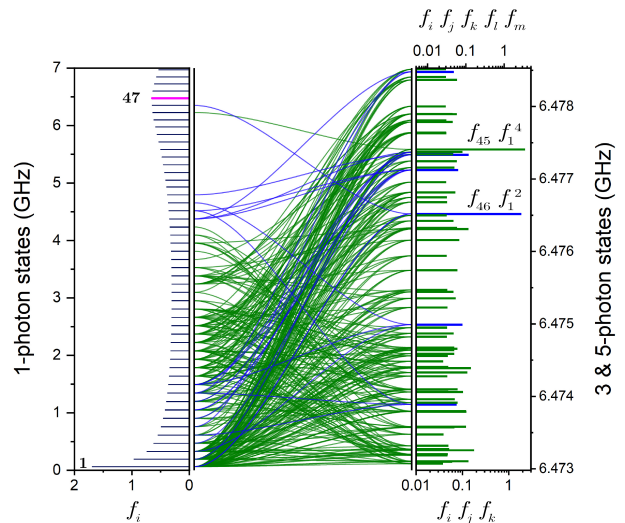


FIG. 4. An example of the states available for the decay of the mode $k = 47$ in device 2a for $\omega_0 \approx \omega_{47}$. The many-body spectrum (right) is obtained by summing all possible combinations of three (blue) and five (green) one-photon frequencies, measured experimentally (left). Each bar's height indicate the one-photon amplitudes f_k (left, see text) and the relative amplitudes of $f_i f_j f_k$ and $f_i f_j f_k f_l f_m$ of 3-photon and 5-photon states, respectively. The frequency range in the right panel equals to the measured half-linewidth of the $k = 47$ mode.

states with energies $\hbar(\omega_i + \omega_j + \omega_k)$ couple relatively uniformly, as estimated by their composite weights $f_i f_j f_k$, and the same applies to five-photon states. The energy uniformity property comes from a small amount of disorder and dispersion in the single-particle spectrum, which breaks the otherwise massive degeneracy of multi-photon states. On reducing the system size (increasing Δ), the many-body spectrum will rapidly become sparse enough to completely suppress the decay. Understanding such energy localization transition in a nearly closed quantum system, originally introduced in the context of Fermi-quasiparticles in a quantum dot²⁸, would be a timely extension of our experiment.

Fig. 4 highlights the contribution of two specific decay channels considered in deriving Eq. 4: $\omega_{47} \rightarrow \omega_{46} + 2\omega_1$ and $\omega_{47} \rightarrow \omega_{45} + 4\omega_1$. Those channels create two and four photons, respectively, at the lowest available frequency $\omega_1/2\pi = 63$ MHz. As the quantum phase-slip itself, such an efficient soft-mode emission has no analogues in semi-classical electromagnetism. For example, the measured decay rates are far too large to be explained by the usual Josephson quartic anharmonicity $\propto \varphi(x=0, t)^4$, on which most of superconducting quantum technology is based. We believe that efficient inelastic scattering of the phase-mode excitations on phase-slips may be an important microscopic process in the dynamics of bosonic superconductor-insulator transitions^{13,29-31}.

Our circuit spectroscopy technique can be readily extended to cover other quantum impurity models. For instance, reducing the junction size (increasing E_C) would

implement the BSG-model. Shunting the weak junction by an inductance would implement a spin-boson model, related to Anderson and Kondo models^{32,33}, in which case a large inelastic scattering cross-section was predicted near the Toulouse point³⁴. Furthermore, rapidly switching the impurity on and off with the flux knob would induce controlled out-of-equilibrium dynamics. Our accurate measurement of $r(\omega)$ can be viewed as an analog quantum computation of a non-trivial many-body quantity. We successfully verified the computation

outcome in the parameter regime available to analytical calculations. The rest of data represents a unique quantum resource for benchmarking numerical methods of many-body physics and testing noisy digital quantum computers, whose initial focus will likely include quantum impurity problems³⁵.

Acknowledgements. We acknowledge useful discussion with I. Protopopov and J. Sau and funding from the US ARO MURI program, US-Israel BSF, and US DOE.

-
- ¹ Akhmadaliev, S. Z. *et al.* Experimental investigation of high-energy photon splitting in atomic fields. *Phys. Rev. Lett.* **89**, 061802 (2002).
- ² Guerreiro, T. *et al.* Nonlinear interaction between single photons. *Phys. Rev. Lett.* **113**, 173601 (2014).
- ³ Blais, A., Girvin, S. M. & Oliver, W. D. Quantum information processing and quantum optics with circuit quantum electrodynamics. *Nat. Phys.* **16**, 247 (2020).
- ⁴ Wallraff, A. *et al.* Strong coupling of a single photon to a superconducting qubit using circuit quantum electrodynamics. *Nature* **431**, 162–167 (2004). URL <http://dx.doi.org/10.1038/nature02851>.
- ⁵ Schuster, D. *et al.* Resolving photon number states in a superconducting circuit. *Nature* **445**, 515–518 (2007).
- ⁶ Astafiev, O. *et al.* Resonance fluorescence of a single artificial atom. *Science* **327**, 840–843 (2010).
- ⁷ Bergeal, N. *et al.* Analog information processing at the quantum limit with a josephson ring modulator. *Nat. Phys.* **6**, 296–302 (2010).
- ⁸ Chang, C. S. *et al.* Observation of three-photon spontaneous parametric down-conversion in a superconducting parametric cavity. *Phys. Rev. X* **10**, 011011 (2020).
- ⁹ Sundaresan, N. M. *et al.* Beyond strong coupling in a multimode cavity. *Phys. Rev. X* **5**, 021035 (2015).
- ¹⁰ Forn-Díaz, P., Lamata, L., Rico, E., Kono, J. & Solano, E. Ultrastrong coupling regimes of light-matter interaction. *Rev. Mod. Phys.* **91**, 025005 (2019).
- ¹¹ Kockum, A. F., Miranowicz, A., De Liberato, S., Savasta, S. & Nori, F. Ultrastrong coupling between light and matter. *Nat Rev Phys* **1**, 19–40 (2019).
- ¹² Nigg, S. E. *et al.* Black-box superconducting circuit quantization. *Phys. Rev. Lett.* **108**, 240502 (2012).
- ¹³ Kuzmin, R. *et al.* Quantum electrodynamics of a superconductor–insulator phase transition. *Nat. Phys.* **15**, 930–934 (2019).
- ¹⁴ Kuzmin, R., Mehta, N., Grabon, N., Mencia, R. & Manucharyan, V. E. Superstrong coupling in circuit quantum electrodynamics. *npj Quantum Inf* **5**, 20 (2019).
- ¹⁵ Koch, J. *et al.* Charge-insensitive qubit design derived from the Cooper pair box. *Phys. Rev. A* **76**, 042319 (2007).
- ¹⁶ Matveev, K. A., Larkin, A. I. & Glazman, L. I. Persistent current in superconducting nanorings. *Phys. Rev. Lett.* **89**, 096802 (2002).
- ¹⁷ Rastelli, G., Pop, I. M. & Hekking, F. W. J. Quantum phase slips in josephson junction rings. *Phys. Rev. B* **87**, 174513 (2013).
- ¹⁸ Averin, D. V., Zorin, A. B. & Likharev, K. K. Bloch oscillations in small Josephson junctions. *Sov. Phys. JETP* **61**, 407–413 (1985).
- ¹⁹ Corlevi, S., Guichard, W., Hekking, F. W. J. & Haviland, D. B. Phase-charge duality of a Josephson junction in a fluctuating electromagnetic environment. *Phys. Rev. Lett.* **97**, 096802 (2006).
- ²⁰ Pechenezhskiy, I. V., Mencia, R. A., Nguyen, L. B., Lin, Y.-H. & Manucharyan, V. E. The superconducting quasicharge qubit. *Nature* **585**, 368 (2020).
- ²¹ Gull, E. *et al.* Continuous-time monte carlo methods for quantum impurity models. *Rev. Mod. Phys.* **83**, 349 (2011).
- ²² Gogolin, A. O., Nersisyan, A. A. & Tsvetlik, A. M. *Bosonization and strongly correlated systems* (Cambridge University Press, 2004).
- ²³ Schmid, A. Diffusion and localization in a dissipative quantum system. *Phys. Rev. Lett.* **51**, 1506 (1983).
- ²⁴ Bulgadaev, S. Phase diagram of a dissipative quantum system. *Pis'ma v Zh. Eksp. Teor. Fiz.* **39**, 264–267 (1984).
- ²⁵ Kane, C. L. & Fisher, M. P. A. Transport in a one-channel luttinger liquid. *Phys. Rev. Lett.* **68**, 1220 (1992).
- ²⁶ Fendley, P., Saleur, H. & Warner, N. P. Exact solution of a massless scalar field with a relevant boundary interaction. *Nucl. Phys. B* **430**, 577–596 (1994).
- ²⁷ Supplementary Materials.
- ²⁸ Altshuler, B. L., Gefen, Y., Kamenev, A. & Levitov, L. S. Quasiparticle lifetime in a finite system: A nonperturbative approach. *Phys. Rev. Lett.* **78**, 2803 (1997).
- ²⁹ Bard, M., Protopopov, I. & Mirlin, A. Decay of plasmonic waves in josephson junction chains. *Phys. Rev. B* **98**, 224513 (2018).
- ³⁰ Wu, H.-K. & Sau, J. D. Theory of coherent phase modes in insulating josephson junction chains. *Phys. Rev. B* **99**, 214509 (2019).
- ³¹ Houzet, M. & Glazman, L. I. Microwave spectroscopy of a weakly pinned charge density wave in a superinductor. *Phys. Rev. Lett.* **122**, 237701 (2019).
- ³² García-Ripoll, J. J., Solano, E. & Martin-Delgado, M. A. Quantum simulation of anderson and kondo lattices with superconducting qubits. *Phys. Rev. B* **77**, 024522 (2008).
- ³³ Le Hur, K. Kondo resonance of a microwave photon. *Phys. Rev. B* **85**, 140506 (2012).
- ³⁴ Goldstein, M., Devoret, M. H., Houzet, M. & Glazman, L. I. Inelastic microwave photon scattering off a quantum impurity in a josephson-junction array. *Phys. Rev. Lett.* **110**, 017002 (2013).
- ³⁵ Bravyi, S. & Gosset, D. Complexity of quantum impurity problems. *Commun. Math. Phys.* **356**, 451–500 (2017).